Electronic Supplementary Material (ESI) for Soft Matter.

Electronic Supplementary Information

Surfactant induced disaggregation of Quinoxaline AIEgen scaffold: Aggregation aptitude in solid and solution state

Sagnik De and Gopal Das*

Department of Chemistry, Indian Institute of Technology Guwahati, Assam 781039, India.

Fax: + 91 361 258 2349; Tel: +91 361258 2313; E-mail: gdas@iitg.ac.in

General Methods and Materials

All reagents, starting materials, solvents, and protein samples were procured from commercial sources and used without further purification. The absorption and emission spectral studies were measured in a Perkin-Elmer Lamda-750 UV-Vis spectrophotometer and Horiba Fluoromax-4 spectrofluorometer respectively. Recording of UV-vis spectra was done in 10 mm path length quartz cuvettes in the range 300-700 nm wavelength, while Fluorescence measurement was done using a 10 mm path length quartz cuvette with a slit width of 3 nm at 25 °C. Chemical shifts of NMR were recorded using a BRUKER-500 MHz and a BRUKER-600 MHz instrument, and reported on a scale in parts per million (ppm). Spin multiplicities from ^{1}H NMR spectra were described using the following abbreviations: s = singlet; d = doublet; t = triplet; m = multiplet. IR spectra with 4000-400 cm^{-1} range were collected using a Perkin Elmer-Spectrum AT-IR spectrometer. Atomic Force Microscope (Make: Oxford, Model: Cypher) and Field Emission Scanning Electron Microscope (Make: Zeiss, Model :- Sigma 300) were used to characterize the topographical and morphological details. The X-ray crystallographic intensity data were collected using a Supernova, a single source at offset, Eos diffractometer using Mo-Kα radiation (λ = 0.71073 Å) equipped with a CCD area detector, and the corresponding data refinement and cell reduction were performed using CrysAlisPro.53 The data integration and reduction were carried out with SAINT and XPREP (ref. 54) software, and multi-scan empirical absorption corrections were applied to the data using the program SADABS.55 All the structures were solved by direct methods using SHELXTL-2014 and 2016 and were refined on F2 by the full-matrix least-squares technique using the SHELXL-2014 and 2016 program packages.56 Hydrogen atoms were geometrically fixed. Structural illustrations are generated using MERCURY 4.1.3 for Windows.

Field Emission Scanning Electron Microscope

FESEM imaging studies were conducted separately with a solution of $\mathbf{L_1}$, $\mathbf{L_2}$, $\mathbf{L_3}$, $\mathbf{L_4}$, and $\mathbf{L_5}$ (1 mM) by changing water fraction from 0% to 100% in THF-water by drop (2 μl) cast method on glass plates covered with Al-foil using Gemini 300 FESEM (Carl Zeiss).

Atomic Force Microscopy

Transformations of L1 due to solvent switching were observed from a drop-cast solution of **L_1**, **L_2**, **L_3**, **L_4**, and **L_5** (10 μM) in a THF-water medium using Asylum Research Cypher (Oxford Instruments).

Dynamic light scattering studies

The particle sizes of **L_1**, **L_2**, **L_3**, **L_4**, and **L_5**, aggregated states were measured by dynamic light scattering (DLS) experiments on Malvern Zetasizer Nano ZS instrument equipped with a 4.0 mW He–Ne laser operating at a wavelength of 633 nm. The samples and the background were measured at room temperature (25 °C). DLS experiments were carried out with optically clear solutions of **L_1** and **L_2** (10 μM) to observe the change in the particle size upon increasing the THF-water fraction. The solution was equilibrated for 120 minutes before taking the measurements.

Detection limit

The detection limit was calculated on the basis of the fluorescence. For this, the fluorescence emission spectra of the probes were measured 10 times. From that, the standard deviation of the blank measurement was calculated. For obtaining the slope, the ratio of the fluorescence emission or absorbance at a specific wavelength was plotted as a concentration of the guest anion. Finally, the detection limit was calculated using the following equation: $\text{Detection limit} = 3\sigma/k$where σ is the standard deviation of the blank measurement, and k is the slope between the ratio of the fluorescence emission or *versus* the respective analyte concentration.

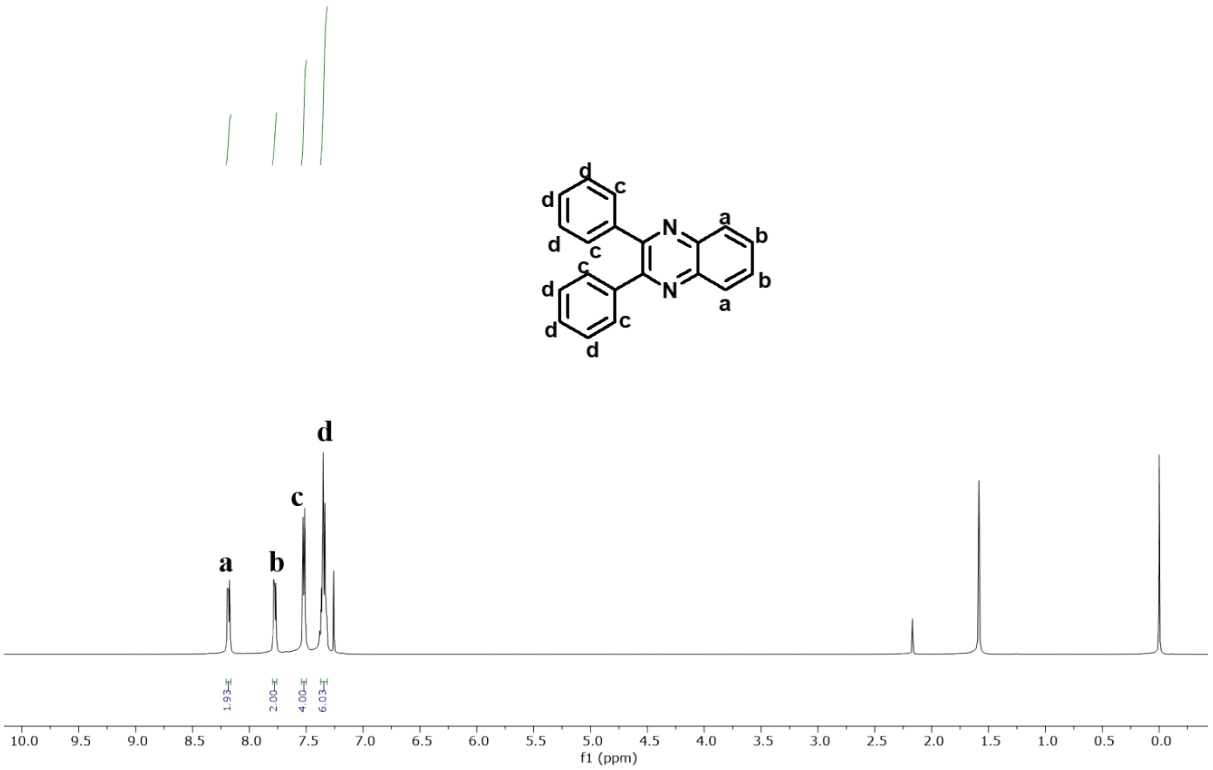

Figure S1: ^{1}H NMR of $\mathbf{L_1}$.

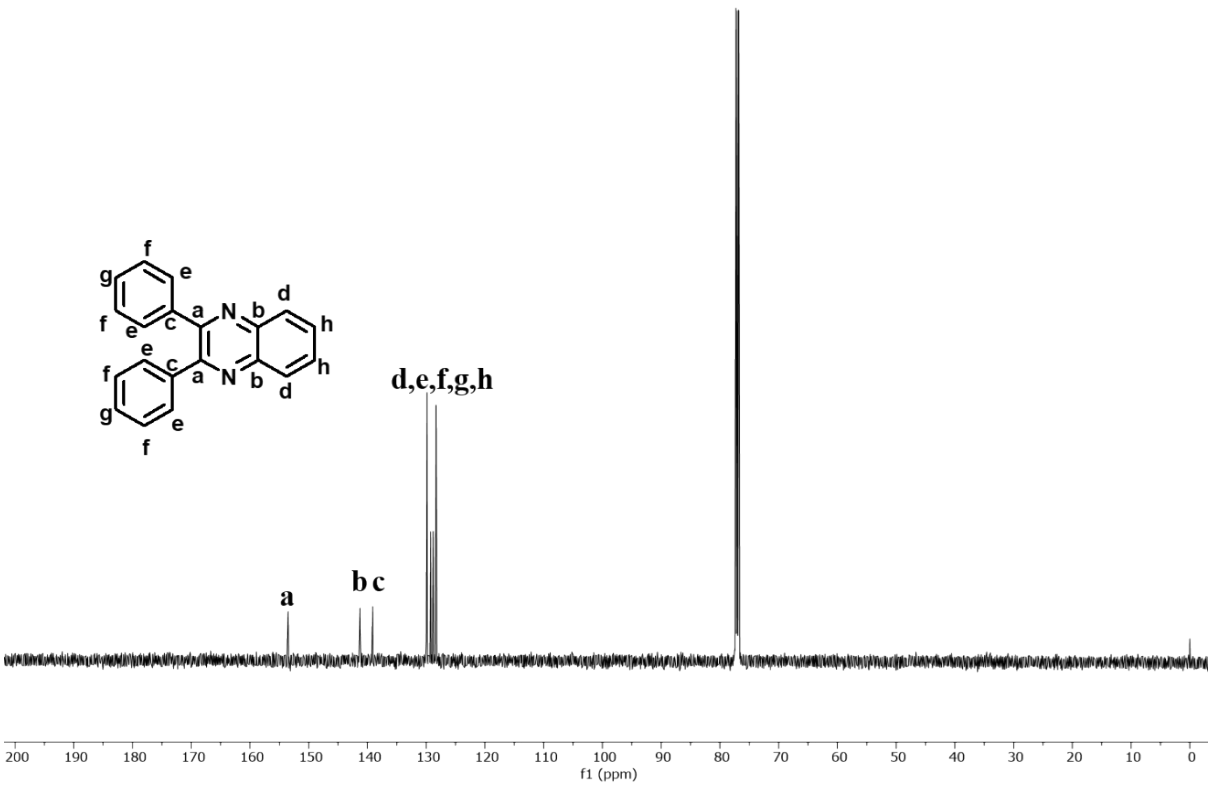

Figure S2: ^{13}C NMR of $\mathbf{L_1}$.

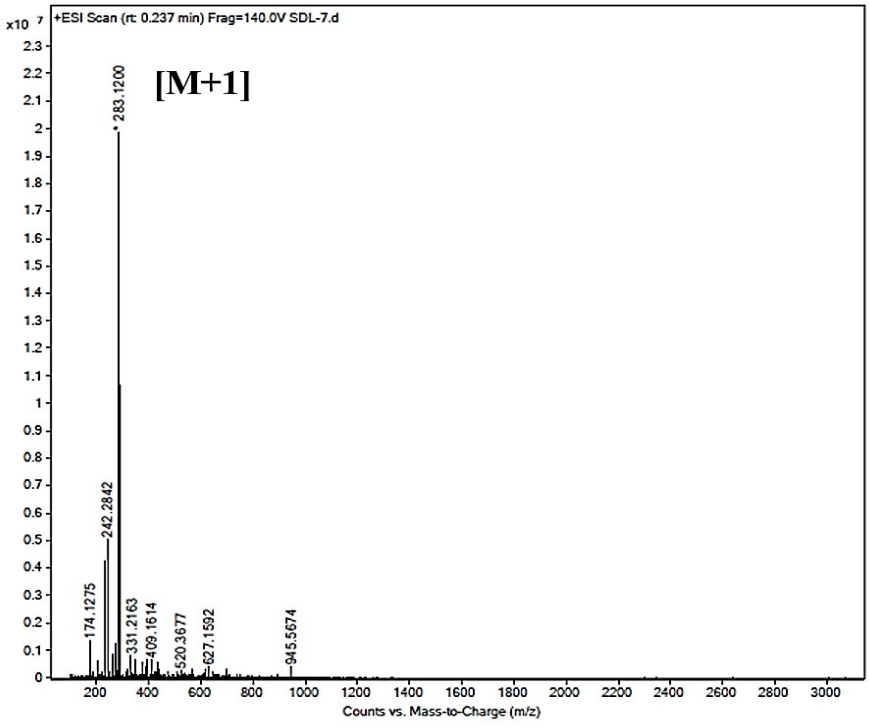

Figure S3: Mass spectra of $\mathbf{L_1}$.

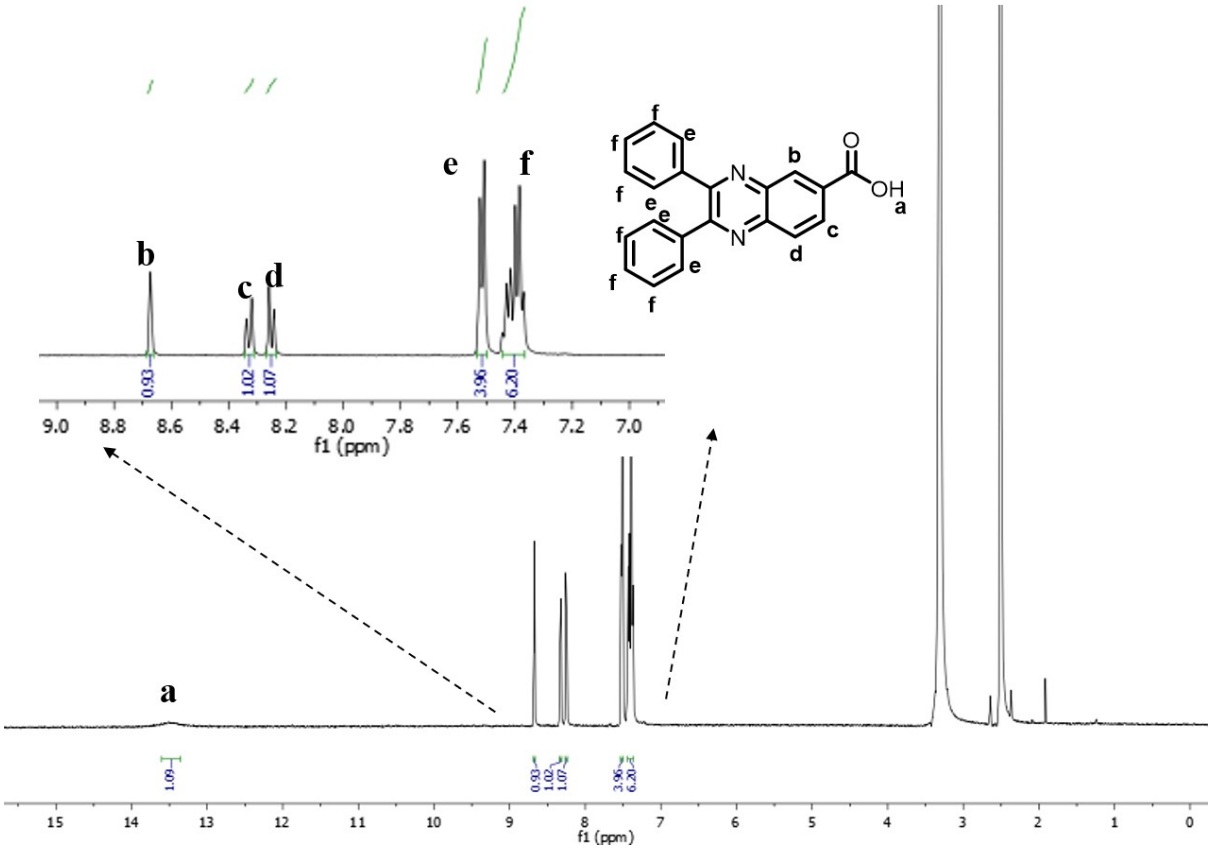

Figure S4: ^{1}H NMR of $\mathbf{L_2}$.

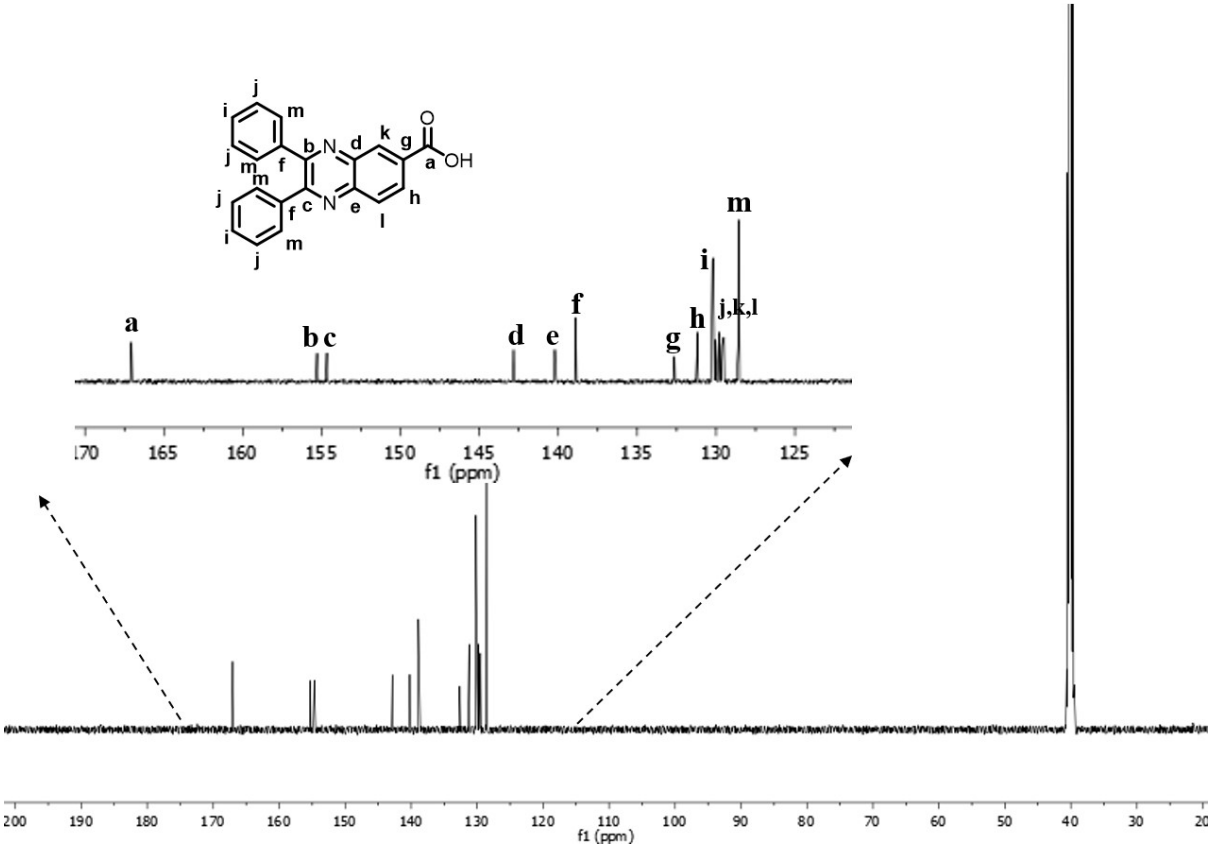

Figure S5: ^{13}C NMR of $\mathbf{L_2}$.

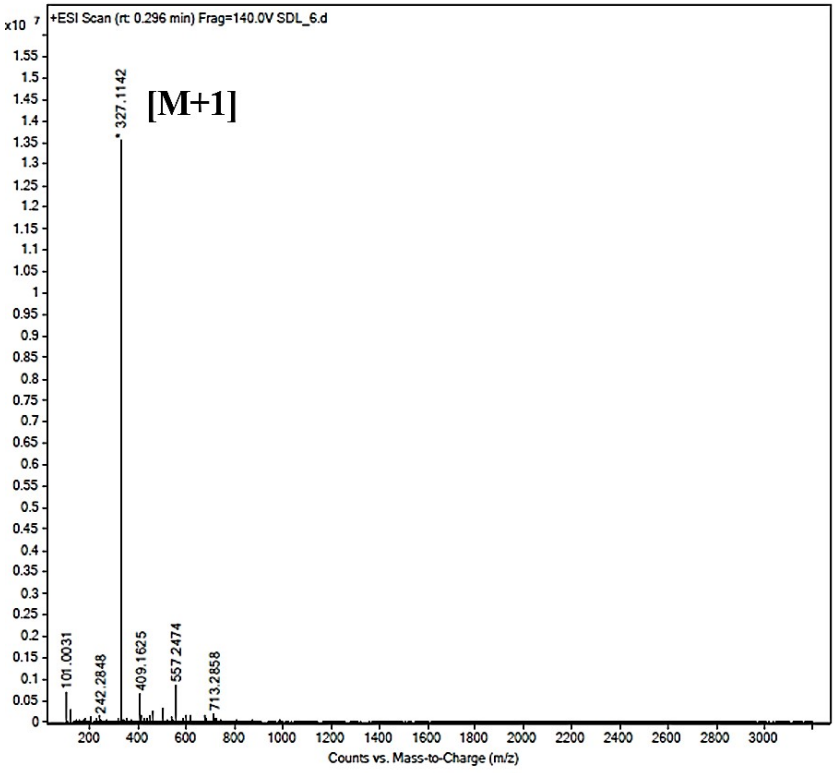

Figure S6: Mass spectra of $\mathbf{L_2}$.

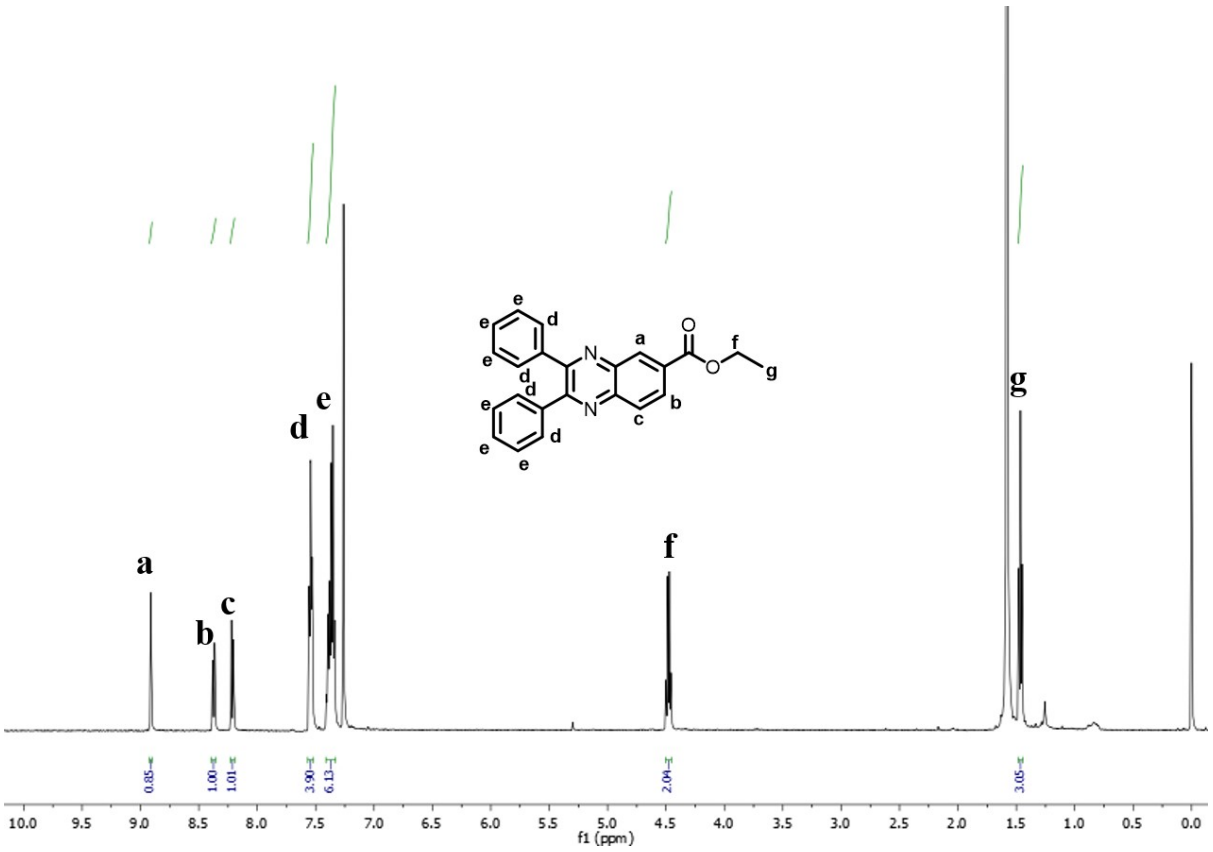

Figure S7: ^{1}H NMR of $\mathbf{L_3}$.

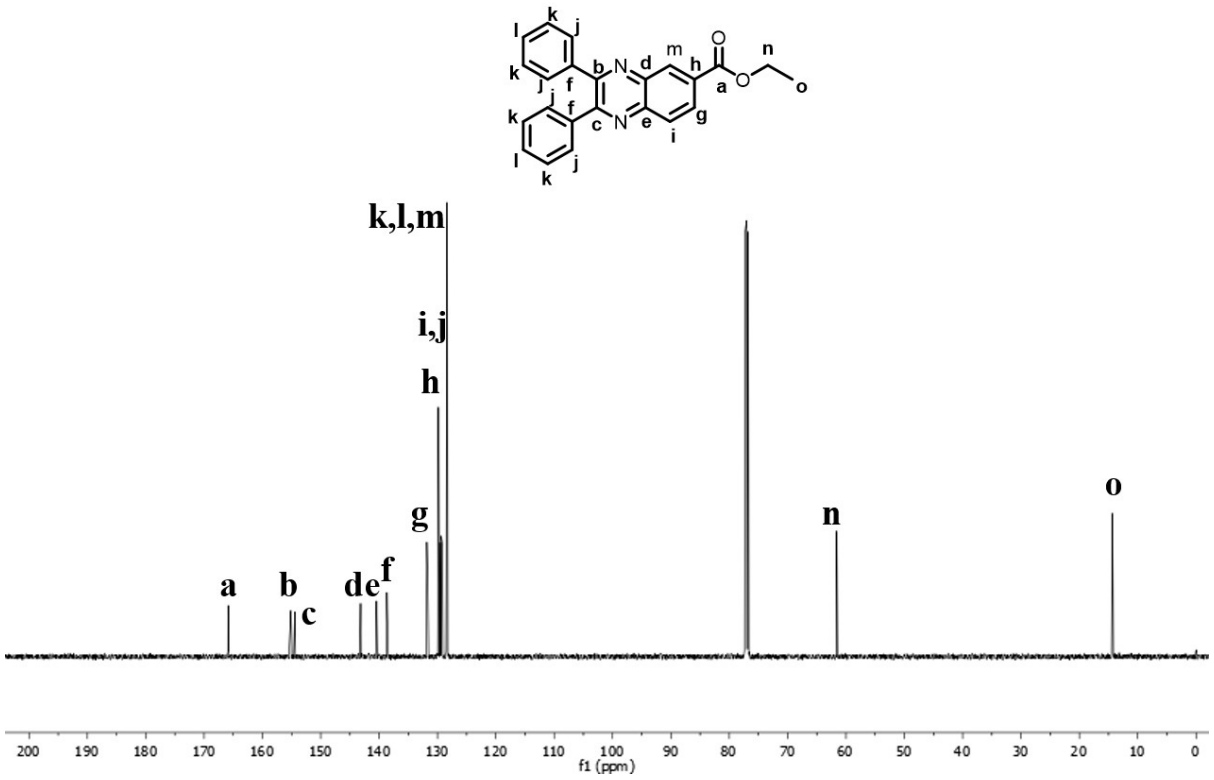

Figure S8: ^{13}C NMR of $\mathbf{L_3}$.

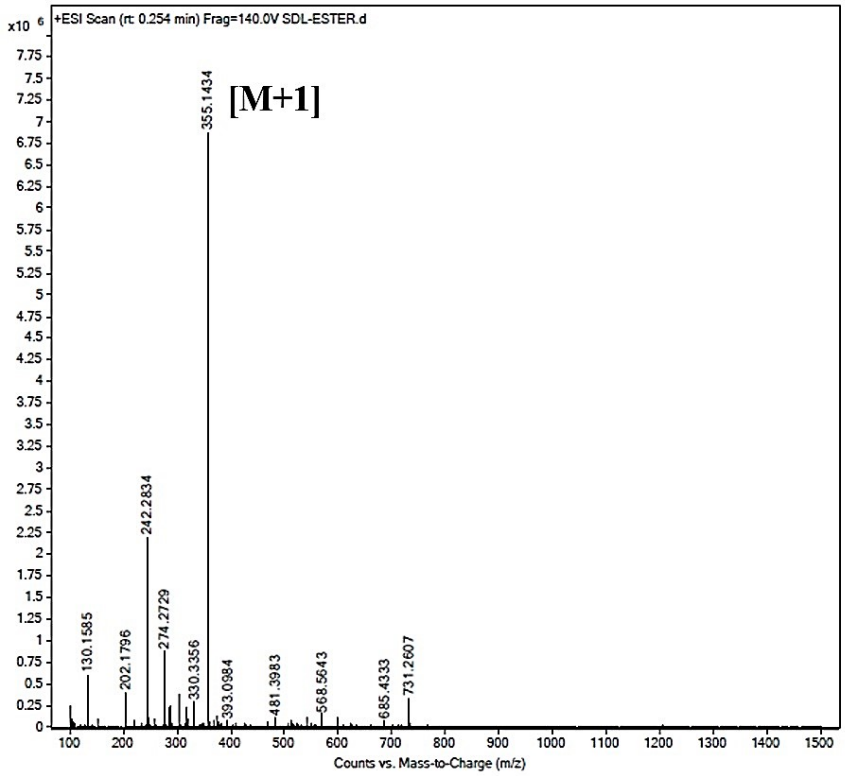

Figure S9: Mass spectra of $\mathbf{L_3}$.

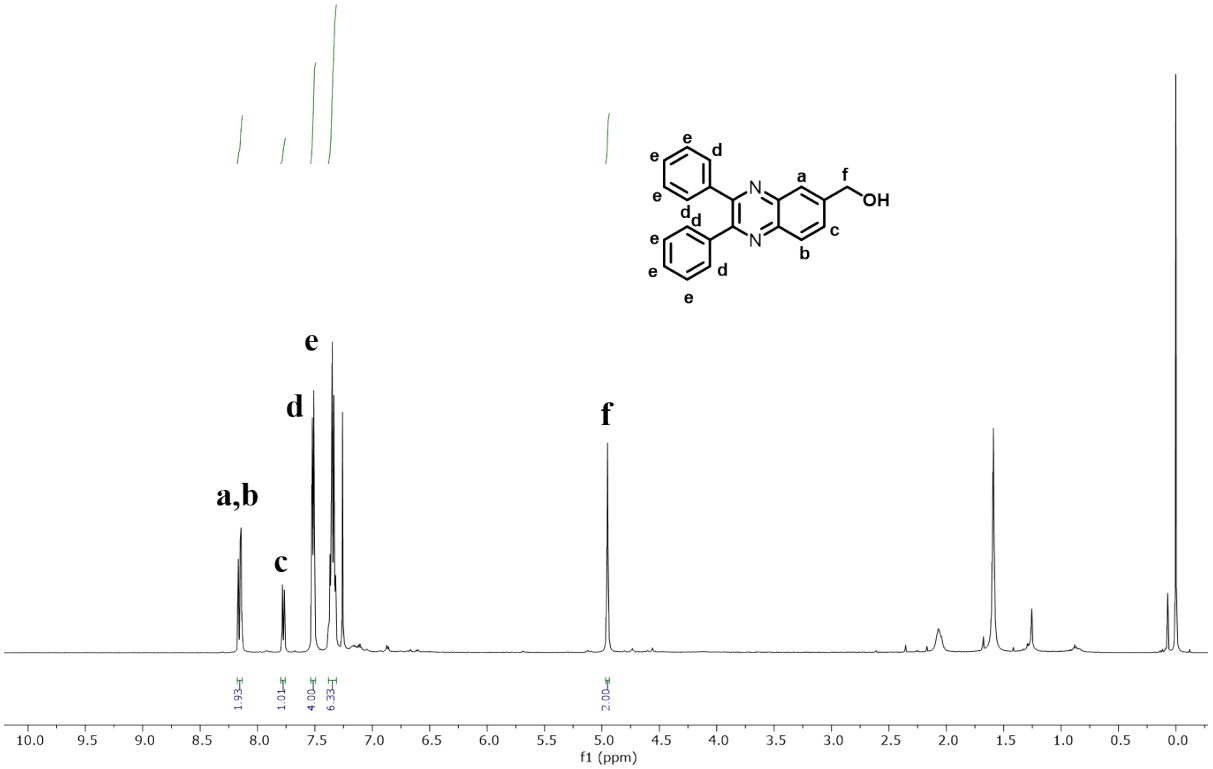

Figure S10: ^{1}H NMR of $\mathbf{L_4}$.

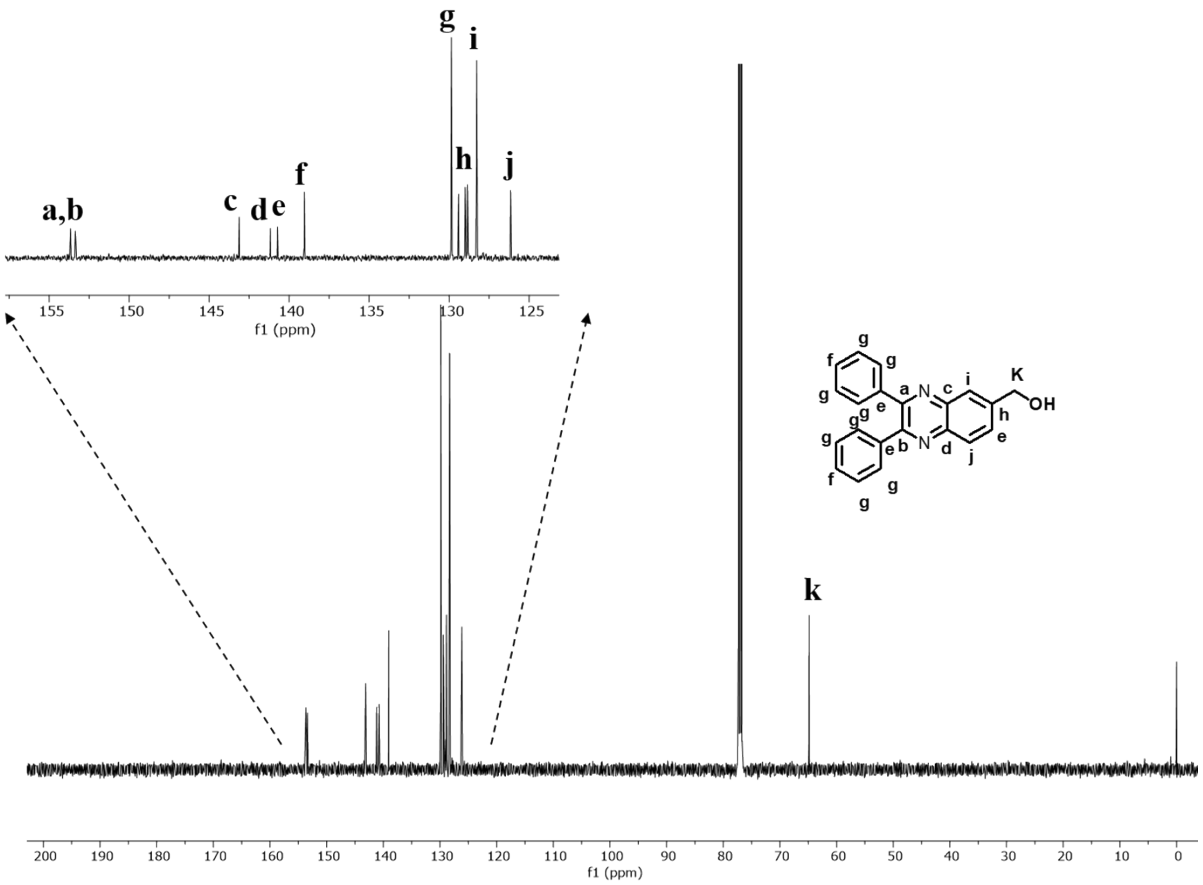

Figure S11: ^{13}C NMR of $\mathbf{L_4}$.

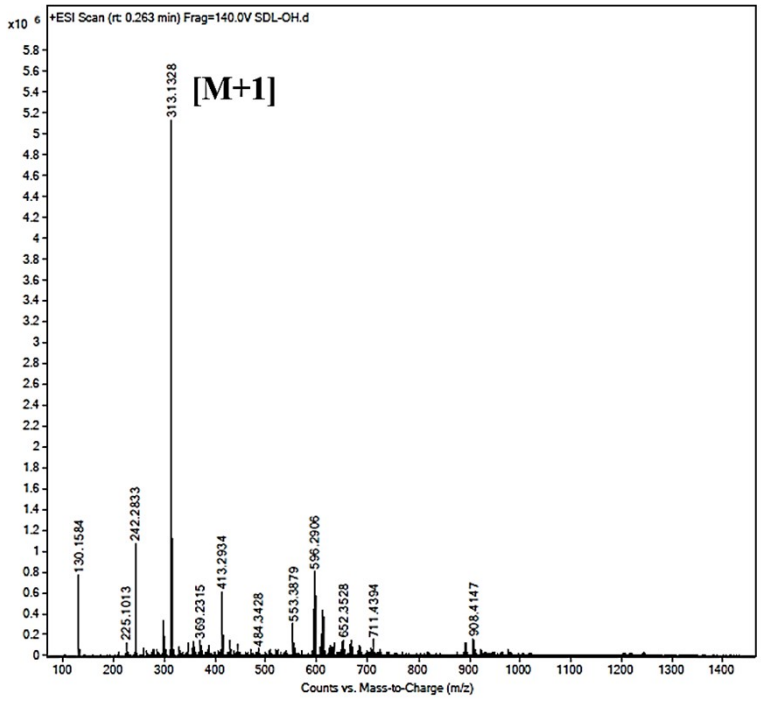

Figure S12: Mass spectra of $\mathbf{L_4}$.

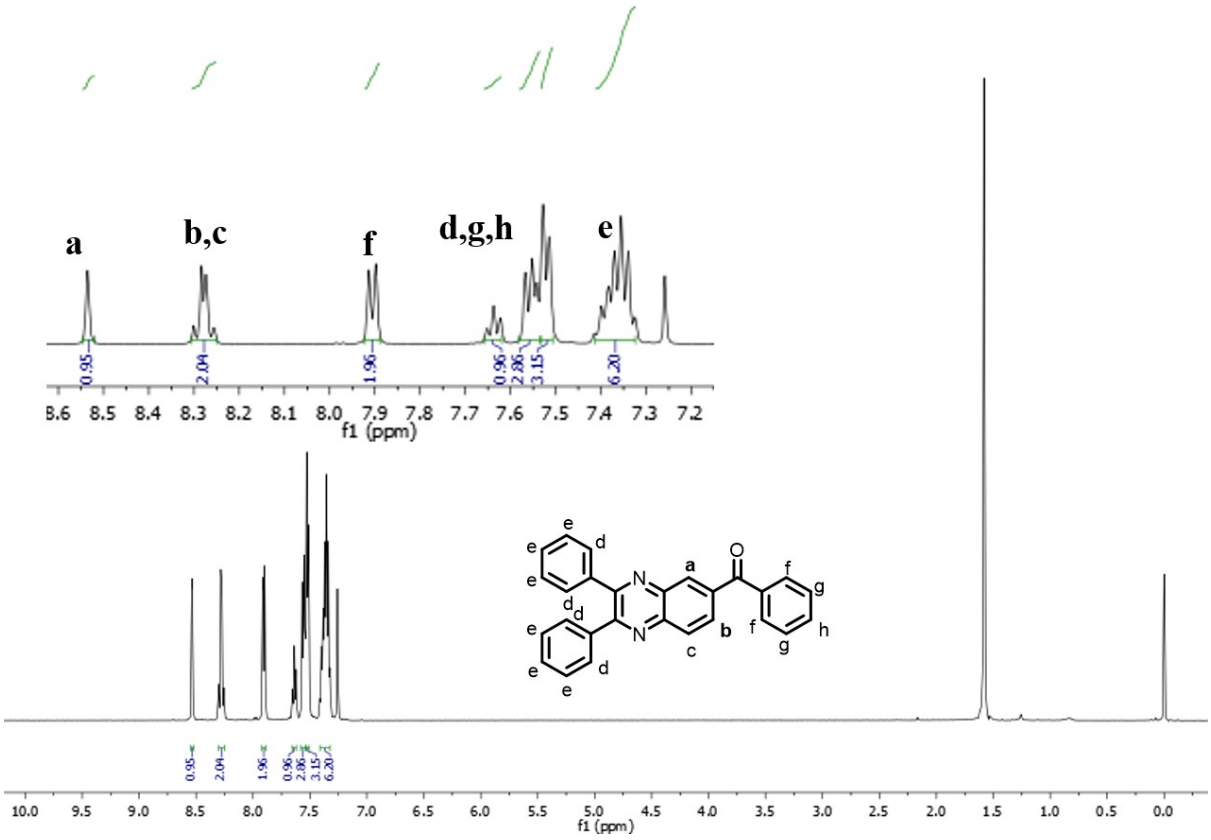

Figure S13: ^{1}H NMR of $\mathbf{L_5}$.

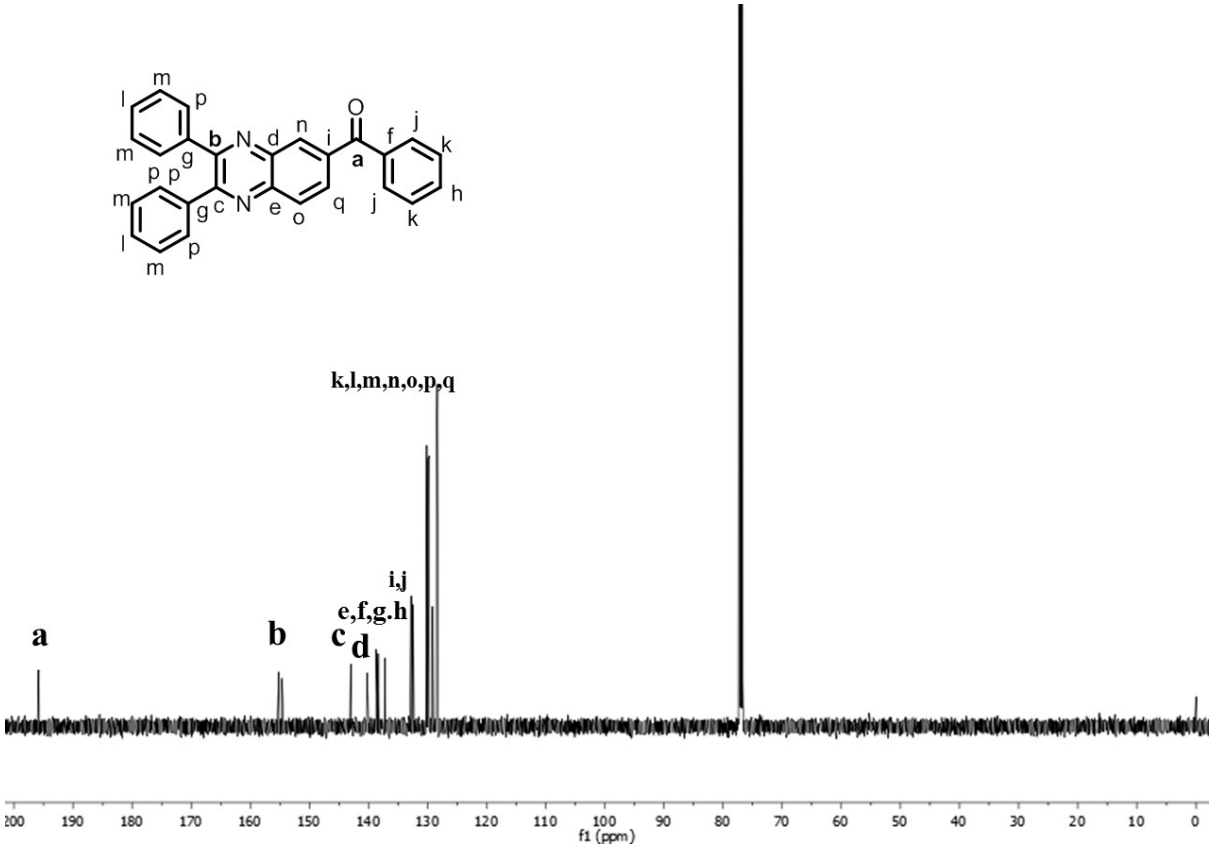

Figure S14: ^{13}C NMR of $\mathbf{L_5}$.

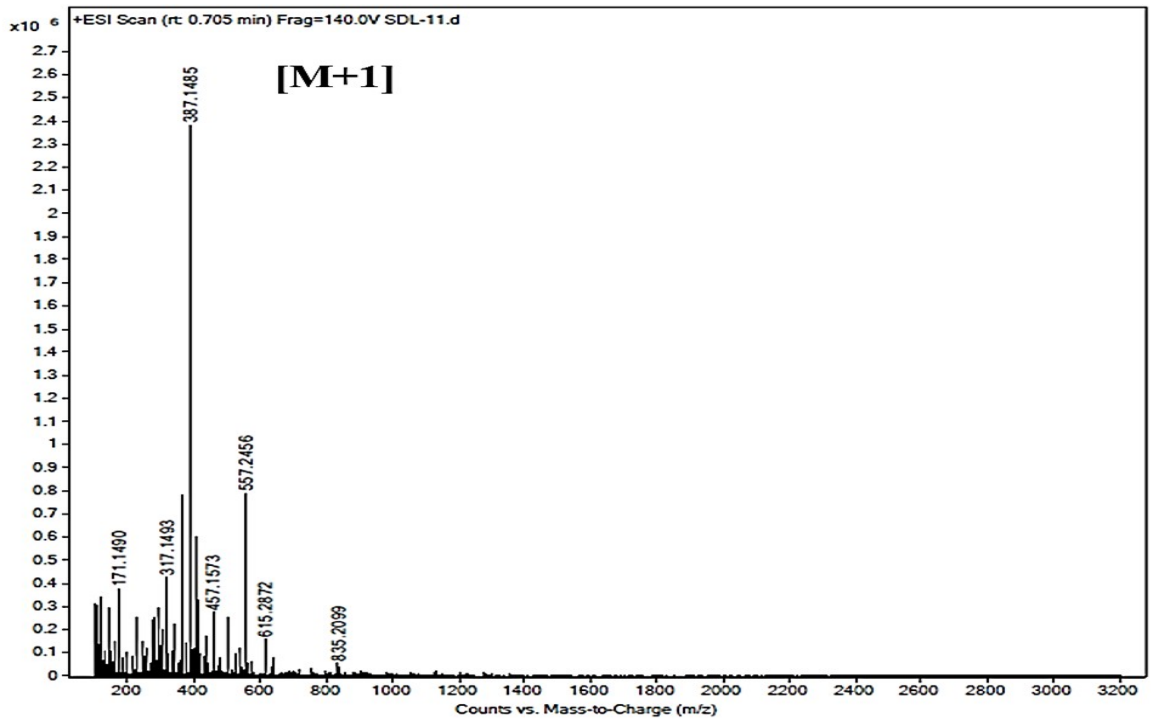

Figure S15: Mass spectra of $\mathbf{L_5}$.

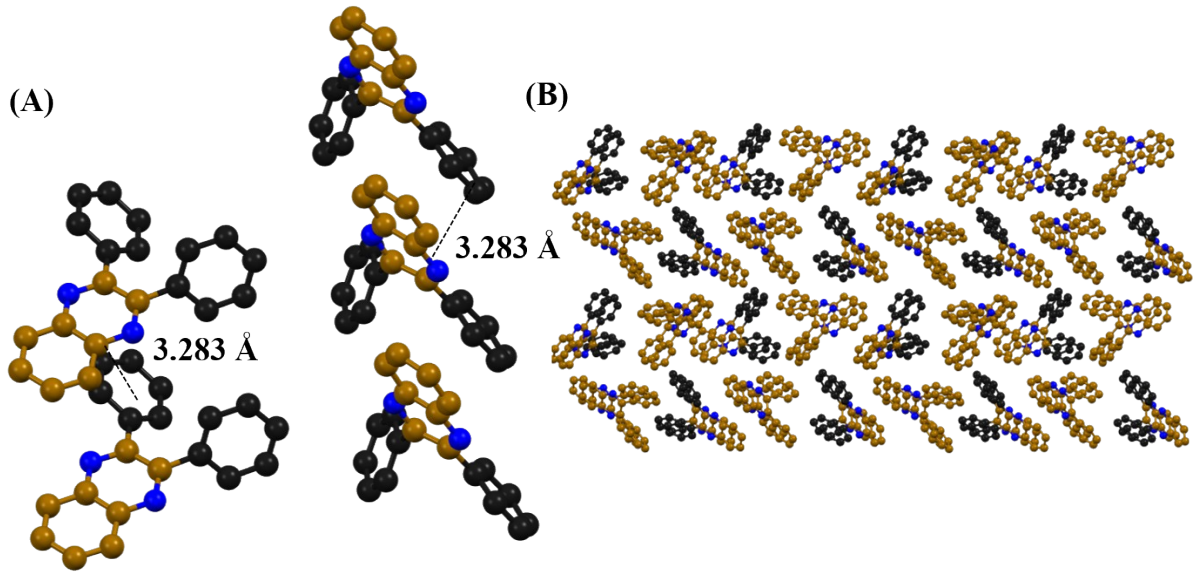

Figure S16: (A) Ligand-ligand interaction (B) Packing arrangement of $\mathbf{L_1}$ in solid state.

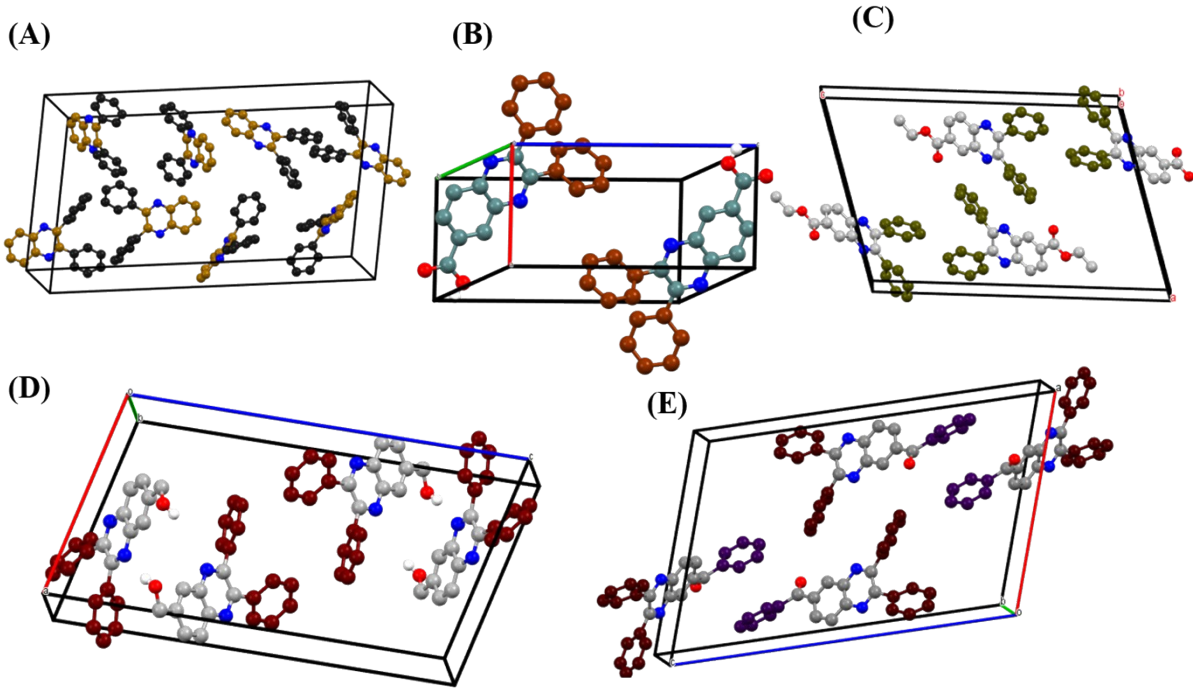

Figure S17: Unit packing diagram (Z values) for $\mathbf{L_1}$, $\mathbf{L_2}$, $\mathbf{L_3}$, $\mathbf{L_4}$ & $\mathbf{L_5}$.

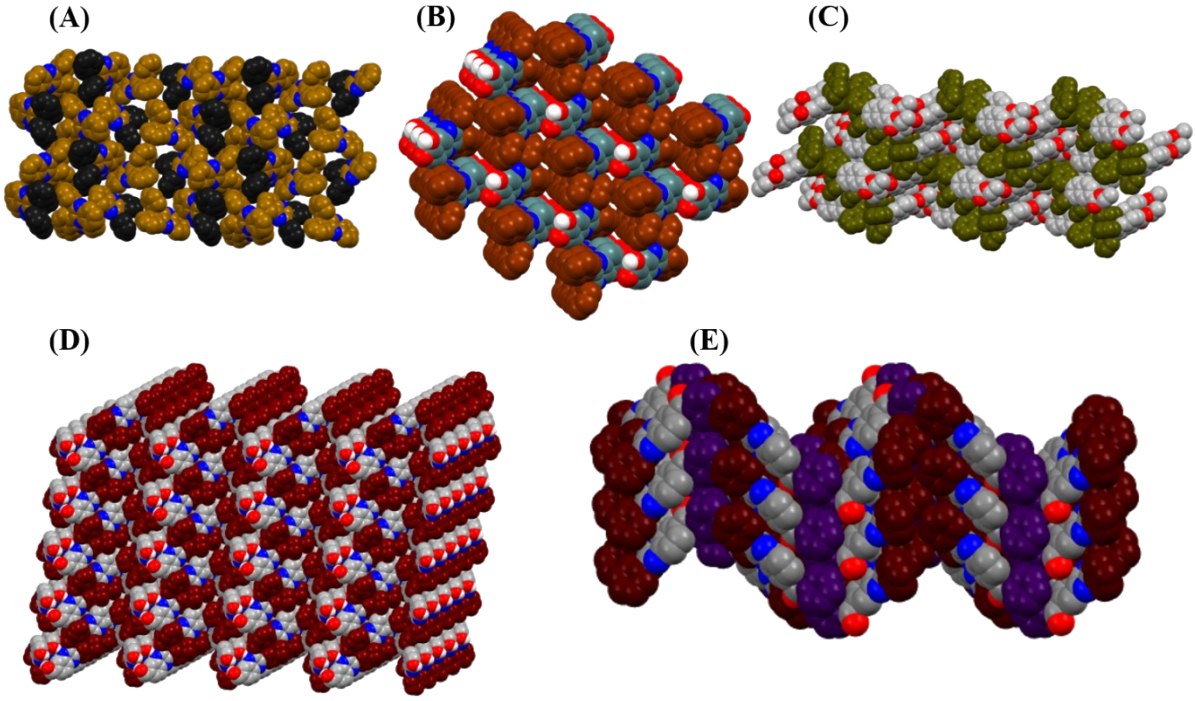

Figure S18: Space fill diagram for (A) L_1, (B) L_2, (C) L_3, (D) L_4 & (E) L_5.

Table 1: Hydrogen bonding distances (Å) and Bond angles (º) in L_2 & L_4.

Compound	D−H···A	d(D···H)/Å	d(H···A)/Å	d(D···A)/Å	<D−H···A/°	Symmetry codes
L_2	O24--H24···O25	0.82	1.79	2.593 (4)	167	2-x, 2-y,-z
	C7--H7N···O24	0.93	2.42	2.736 (5)	167	
L_4	O24—H15···N1	0.82	2.01	2.825(3)	170	3/2-x, -1/2+y,1/2-z
	C20—H11···O24	0.93	2.53	2.853(3)	100	

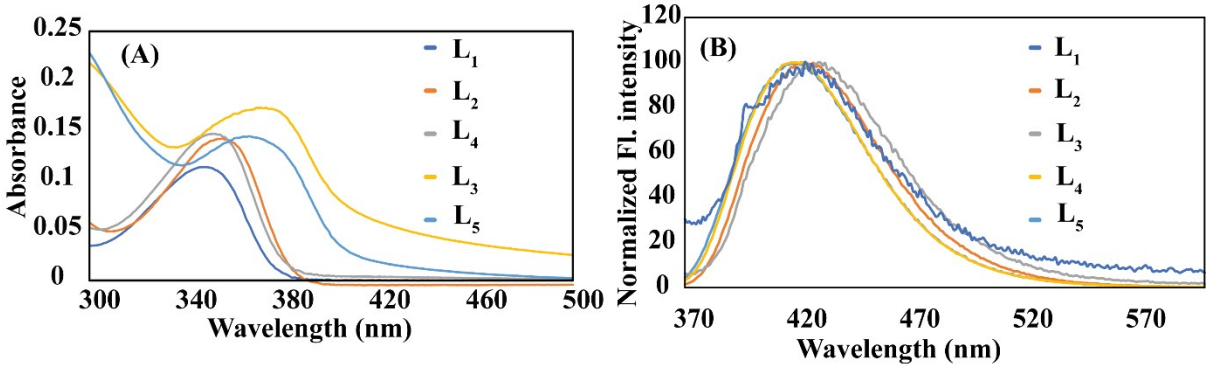

Figure S19: (A) UV-vis spectra of L_1, L_2, L_3, L_4 & L_5 in water. (B) Emission spectra of L_1, L_2, L_3, L_4 & L_5 congeners in water excitation: 350 nm, in all cases).

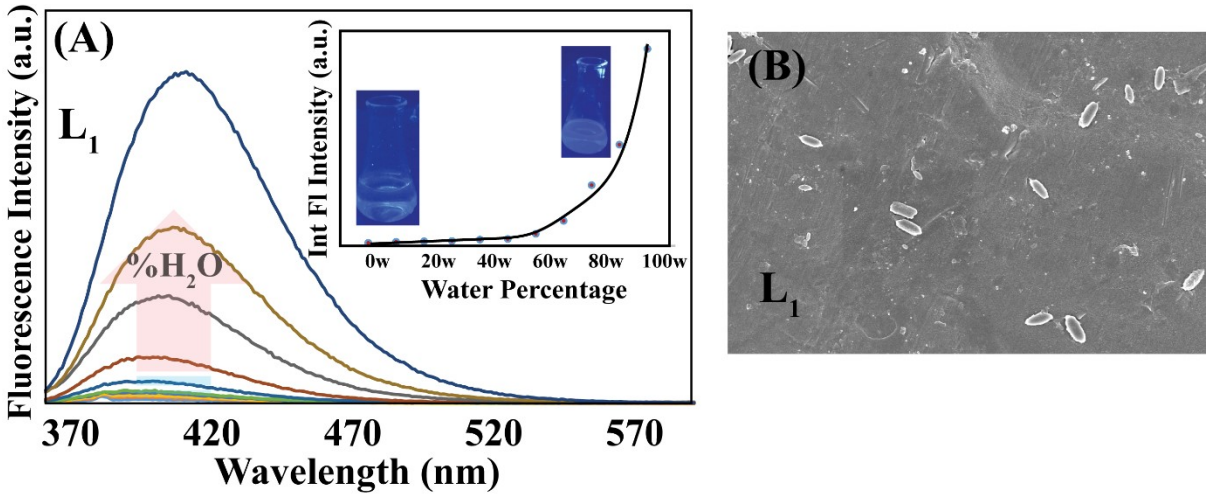

Figure S20: (A) Emission spectra of L_1 depicting AIEgenic behaviour. (B) FESEM image of L_1 in water (excitation: 350 nm).

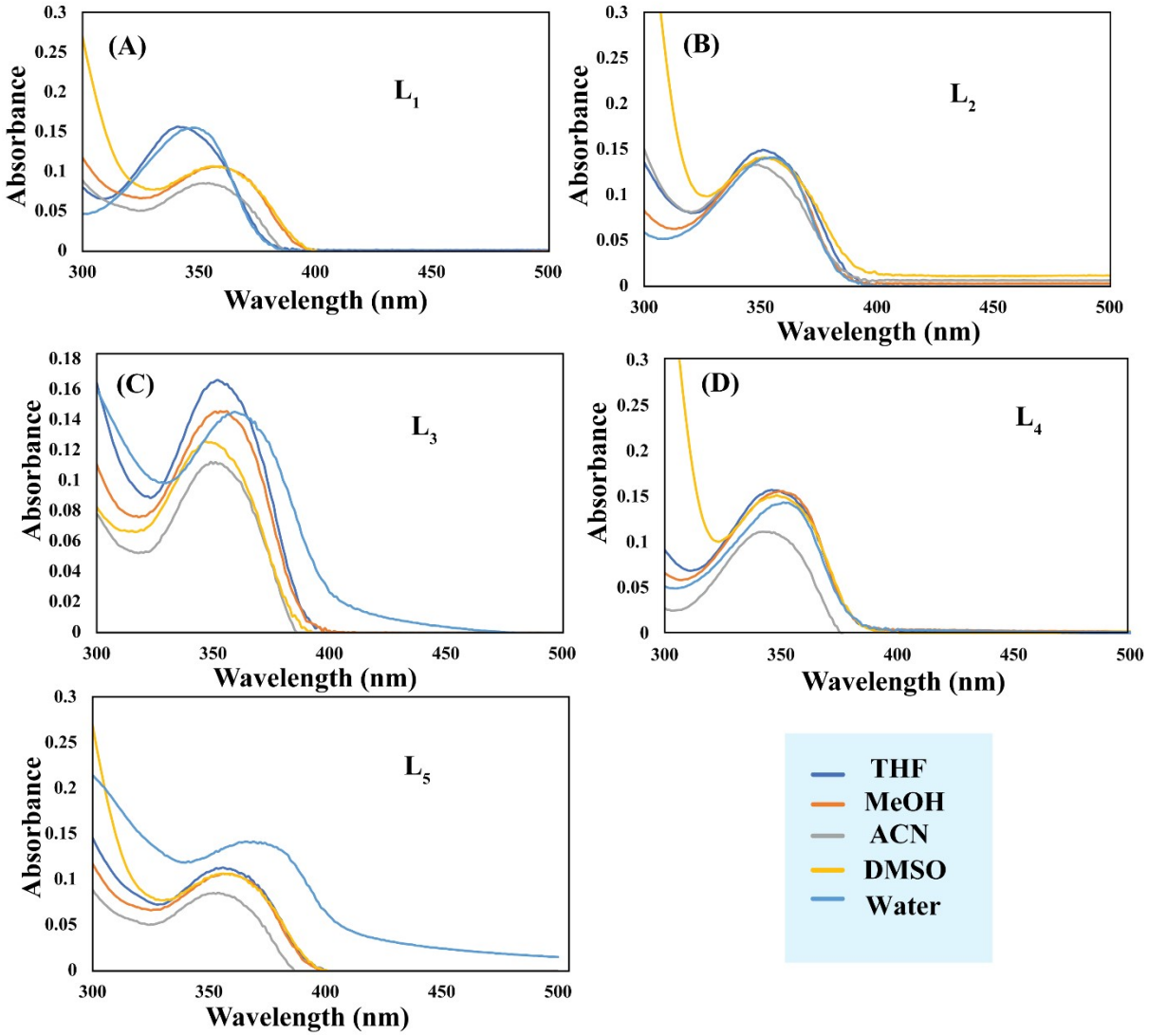

Figure S21: Absorption Spectres regarding the effect of solvent variation $\mathbf{L_1}$, $\mathbf{L_2}$, $\mathbf{L_3}$, $\mathbf{L_4}$ and $\mathbf{L_5}$(10 μM).

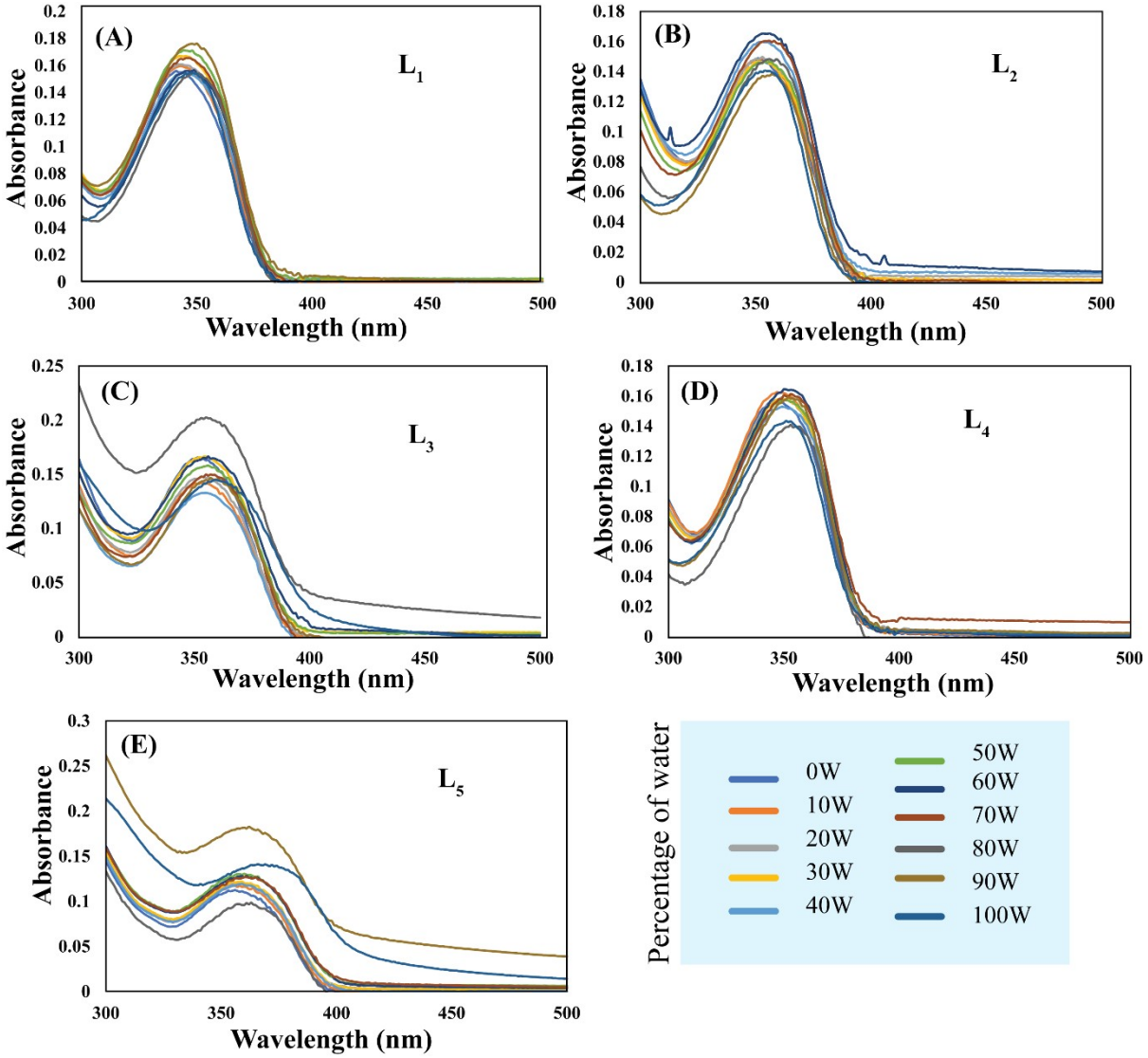

Figure S22: Absorption Spectres regarding the effect of water fraction variation in THF $\mathbf{L_1}$, $\mathbf{L_2}$, $\mathbf{L_3}$, $\mathbf{L_4}$ and $\mathbf{L_5}$ (10 μM).

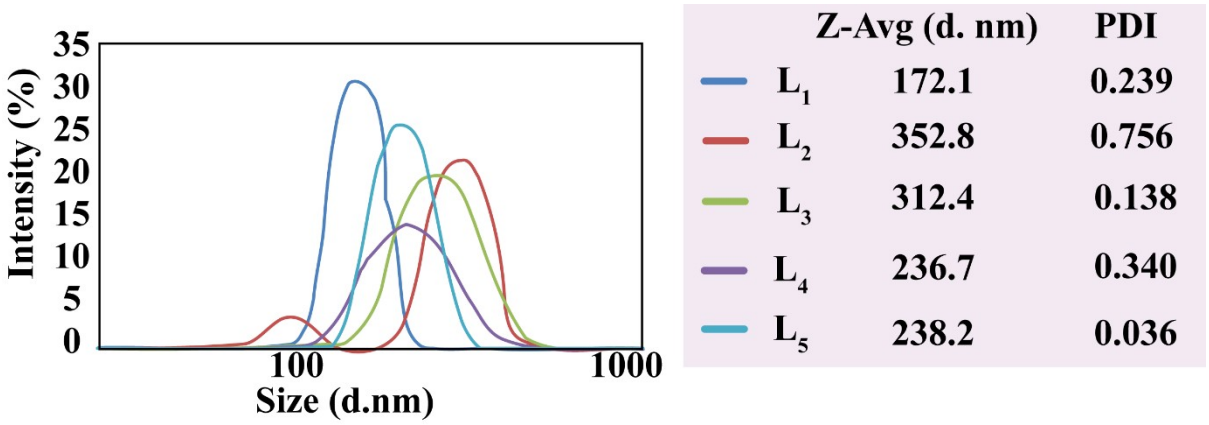

Figure S23: DLS output of L_1, L_2, L_3, L_4 & L_5 (diameter in nanometres is expressed as d. nm).

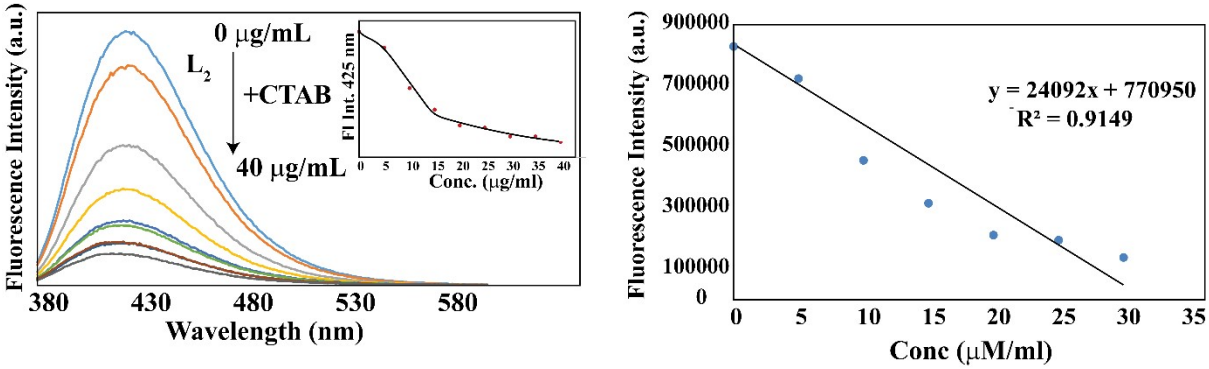

Figure S24: (A) Emission spectra of titration with the gradual addition of CTAB, (inset: Graph depicting fall in fluorescence intensity w.r.t increase in CTAB concentration (A)Plot from the titration and determination of slope for L.O.D. calculation (excitation: 350 nm).

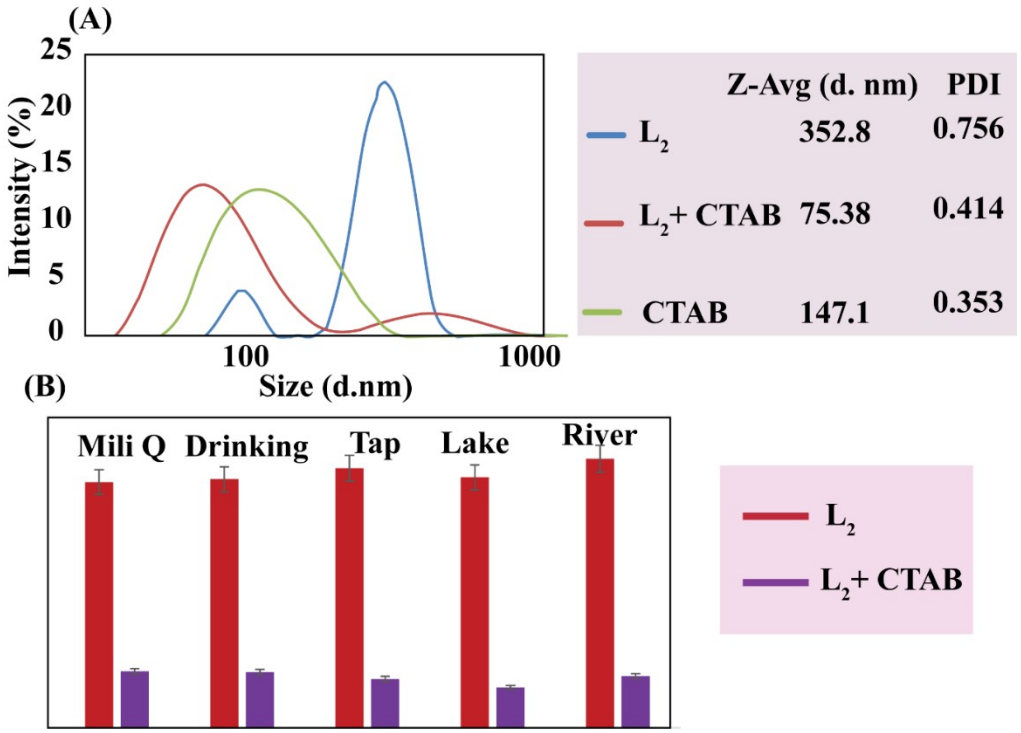

Figure S25: (A) DLS output of $\mathbf{L_2}$ in presence and absence of CTAB (diameter in nanometres is expressed as d. nm). (B) Real water samples as a medium for chemo sensing of CTAB with $\mathbf{L_2}$(excitation: 350 nm).

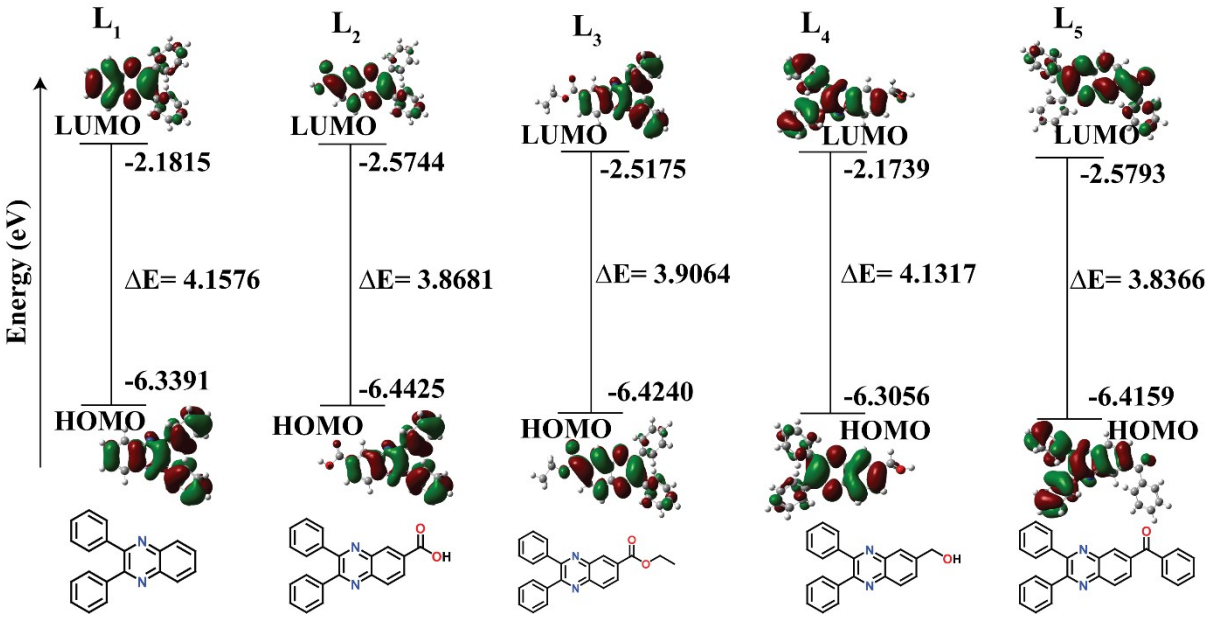

Figure S26: Output of DFT calculation on L_1, L_2, L_3, L_4, and L_5, Density functional theory (DFT) calculations were calculated with the B3LYP/6-31G(d,p) method basis set using the Gaussian 09 program. The CPCM solvent model has been implemented using water as a solvent during calculation.